Centrality Dependence of Multistrange Particle Production in Heavy-Ion Collisions at High Energies

Carlos Merino

Dept. of Particle Physics – Physics Faculty

Galician Institute of High-Energy Physics (IGFAE)

University of Santiago de Compostela – USC, Galiza (Spain)

in collaboration with G.H. Arakelyan and Yu.M. Shabelski

carlos.merino@usc.es

Carlos Merino at HYP2022
14th International Conference on Hypernuclear and Strange Particle Physics
Prague, Czech Republic, June 29th, 2022

1/27

Aim:

The **multistrange baryons and antibaryons** are a valuable probe in understanding the particle production mechanism in high energy collisions.

We compare the **experimental ratios of multistrange to strange antibaryon production on nuclear targets at the energy region from SPS to LHC,** with the **corresponding results** obtained in the frame of the **Quark-Gluon String Model (QGSM).**

Carlos Merino at HYP2022
14th International Conference on Hypernuclear and Strange Particle Physics
Prague, Czech Republic, June 29th, 2022

2/27

A **remarkable** feature of strangeness production is that the production of each additional *s* quark featuring in the secondary baryons, is affected by one universal strangeness suppression factor, λ_s:

$$\lambda_s = \frac{B(qqs)}{B(qqq)} = \frac{B(qss)}{B(qqs)} = \frac{B(sss)}{B(qss)} \, ,$$

together with some simple quark combinatorics (B's are production yields).

Let us define:

$$R(\bar{\Xi}^+/\bar{\Lambda}) = \frac{dn}{dy}(A + B \to \bar{\Xi}^+ + X)/\frac{dn}{dy}(A + B \to \bar{\Lambda} + X),$$

$$R(\bar{\Omega}^+/\bar{\Lambda}) = \frac{dn}{dy}(A + B \to \bar{\Omega}^+ + X)/\frac{dn}{dy}(A + B \to \bar{\Lambda} + X).$$

The produced antihyperons $\bar{\Xi}^+$ and $\bar{\Omega}^+$ contain antiquarks newly produced during the collision.

These ratios are reasonably described by the QGSM when a relatively small number of incident nucleons participate in the collision (nucleon-nucleus, or peripheral nucleus-nucleus collisions).

Secondary Production in QGSM:
Inclusive Spectra in pp, pA, and AA collisions

The QGSM is based on Dual Topological Unitarization, Regge phenomenology, and nonperturbative features of QCD.

In QGSM, high energy interactions are considered to proceed via the exchange of one or several Pomerons. The cut of part of those Pomerons determines inelastic scattering amplitude, through the decay of the resulting quark-gluon strings.

The QGSM successfully describes multiparticle production in hadron-hadron, hadron-nucleus and nucleus-nucleus collisions, for a wide energy region.

Carlos Merino at HYP2022
14th International Conference on Hypernuclear and Strange Particle Physics
Prague, Czech Republic, June 29th, 2022

5/27

For a nucleon target, the inclusive rapidity, y, or Feynman-x, x_F, spectrum of a secondary hadron h has the form

$$\frac{dn}{dy} = \frac{x_E}{\sigma_{inel}} \cdot \frac{d\sigma}{dy} = \sum_{n=1}^{\infty} \omega_n \cdot \Phi_n^h(x)$$

where the functions $\Phi_n^h(\mathbf{x})$ determine the contribution of diagrams with n cut Pomerons.

Carlos Merino at HYP2022
14th International Conference on Hypernuclear and Strange Particle Physics
Prague, Czech Republic, June 29th, 2022

6/27

For pp collisions:

$$\phi_n^h(x) = f_{qq}^h(x_+, n) \cdot f_q^h(x_-, n) + f_q^h(x_+, n) \cdot f_{qq}^h(x_-, n) + 2(n-1) f_s^h(x_+, n) \cdot f_s^h(x_-, n) \ ,$$

$$x_\pm = \frac{1}{2} \left[\sqrt{4m_T^2/s + x^2} \pm x \right] \ ,$$

where $f_{qq}, \ f_q, \ \text{and} \ f_s$ are the contributions of diquarks, valence quarks, and sea quarks, respectively.

Carlos Merino at HYP2022
14th International Conference on Hypernuclear and Strange Particle Physics
Prague, Czech Republic, June 29th, 2022

7/27

The **inclusive spectrum of a secondary hadron h, is** determined by the **convolution** of the diquark, valence quark, and sea quark distributions, **u(x, n)**, in the incident particles, **with** the fragmentation functions, **Gʰ(z)**, of quarks and diquarks into the secondary hadron **h**.

$$f_q^h(x_+, n) = \int_{x_+}^{1} u_q(x_1, n) \cdot G_q^h(x_+/x_1) dx_1 \quad .$$

Both the distributions and the fragmentation functions are constructed using the Reggeon counting rules.

In the case of **interaction with a nuclear target**, the multiple scattering theory **(Gribov-Glauber theory)** is used.

In **pA collisions** one should consider that one or several Pomeron cuts in each of the blobs of the proton-nucleon inelastic interaction.

It is also essential to take into account all diagrams with every possible Pomeron configuration, and its corresponding permutations.

For **AA collisions**, the rigid target approximation of the **Glauber theory** is used.

The **superposition picture of QGSM** gives a **reasonable description of** the inclusive spectra on nuclear targets **at energies** $\sqrt{s} = 14 - 30\ GeV$.

Carlos Merino at HYP2022
14th International Conference on Hypernuclear and Strange Particle Physics
Prague, Czech Republic, June 29th, 2022

9/27

At RHIC, the experimental data for Au+Au collisions give clear evidence of suppression effects that reduce the midrapidity inclusive density by about a factor two, when compared with the superposition picture.

This reduction is explained by the inelastic screening corrections, connected to multipomeron interactions.
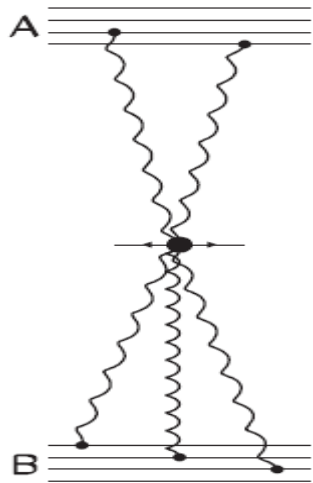
Inclusive cross-section corresponding to the diagram with fusion of several Pomerons.

In order to account for the screening effects in the QGSM, one effectively considers the maximal number of Pomerons, n_{max}, emitted by one nucleon in the central region.

In QGSM, the maximal number of Pomerons, n_{max}, grows with the initial energy of the collision.

By taking this approximation, QGSM calculations become very similar to those in the percolation approach.

Comparison of QGSM Results with experimental data:

1. Fixed Target Energy Data

2. Star Collaboration Data

3. LHC Data

Carlos Merino at HYP2022
14th International Conference on Hypernuclear and Strange Particle Physics
Prague, Czech Republic, June 29th, 2022

12/27

1. Fixed Target Energy Data

We compare with the experimental data by the NA57 Collaboration on proton and hyperon production in p+Be and p+Pb collisions at 158 GEV/c per nucleon (J. Phys. G32 (2006), 427).

In the case of Pb+Pb collisions at 158 GeV/c per nucleon, we compare with the data measured by NA49 (Phys. Rev. C80 (2009), 034906), NA57 (Phys. Lett. B595 (2004), 68), and WA97 (Phys. Lett. B449 (1999), 401) collaborations.

Carlos Merino at HYP2022
14th International Conference on Hypernuclear and Strange Particle Physics
Prague, Czech Republic, June 29th, 2022

13/27

Process	dn/dy, $|y| \leq 0.5$ (Experimental Data)	dn/dy (QGSM)
$p + Be \rightarrow \Lambda$	$0.0334 \pm 0.0005 \pm 0.003$	0.0357
$p + Be \rightarrow \overline{\Lambda}$	$0.011 \pm 0.0002 \pm 0.001$	0.0128
$p + Pb \rightarrow \Lambda$	$0.060 \pm 0.002 \pm 0.006$	0.0678
$p + Pb \rightarrow \overline{\Lambda}$	$0.015 \pm 0.001 \pm 0.002$	0.0173
$p + Be \rightarrow \Xi^-$	$0.0015 \pm 0.0001 \pm 0.0002$	0.00261
$p + Be \rightarrow \overline{\Xi}^+$	$0.0007 \pm 0.0001 \pm 0.0002$	0.00113
$p + Pb \rightarrow \Xi^-$	$0.0030 \pm 0.0002 \pm 0.0003$	0.00336
$p + Pb \rightarrow \overline{\Xi}^+$	$0.0012 \pm 0.0001 \pm 0.0001$	0.00113
$p + Be \rightarrow \Omega^-$	$0.00012 \pm 0.00006 \pm 0.00002$	0.000143
$p + Be \rightarrow \overline{\Omega}^+$	$0.00004 \pm 0.00002 \pm 0.00001$	0.0000453
$p + Pb \rightarrow \Omega^-$	$0.00022 \pm 0.00008 \pm 0.00003$	0.000184
$p + Pb \rightarrow \overline{\Omega}^+$	$0.00005 \pm 0.00003 \pm 0.00002$	0.000058

The experimental data by the NA57 Collaboration on inclusive densities dn/dy of hyperon production in p+Be and p+Pb central lyl≤0.5 collisions at proton-nucleon 158 GeV/c, together with the results of the QGSM calculations (λ_s=0.32) → The consistent agreement with the experimental data is apparent.

Process	Centrality	dn/dy, $\|y\| \leq 0.4$ (Experimental Data)	dn/dy (QGSM)
Pb+Pb $\to p$	0−5%	29.6 ± 0.9 [76]	30.29
Pb+Pb $\to \Lambda$	0−10%	$9.5 \pm 0.1 \pm 1.0$ [79, 81]	6.64
Pb+Pb $\to \Lambda$	0−10%	$10.9 \pm 1.0 \pm 1.3$ [77, 81]	
Pb+Pb $\to \Lambda$	0−10%	13.7 ± 0.9 [81, 32]	
Pb+Pb $\to \overline{\Lambda}$	0−10%	$1.24 \pm 0.03 \pm 0.13$ [79, 81]	1.65
Pb+Pb $\to \overline{\Lambda}$	0−10%	$1.62 \pm 0.16 \pm 0.2$ [77, 81]	
Pb+Pb $\to \overline{\Lambda}$	0−10%	1.8 ± 0.2 [81, 32]	
Pb+Pb $\to \Xi^-$	0−5%	$2.08 \pm 0.09 \pm 0.21$ [81, 83]	1.458
Pb+Pb $\to \overline{\Xi}^+$	0−5%	$0.51 \pm 0.04 \pm 0.05$ [81, 83]	0.482
Pb+Pb $\to \Xi^-$	0−10%	1.5 ± 0.01 [81, 32]	1.34
Pb+Pb $\to \overline{\Xi}^+$	0−10%	0.37 ± 0.06 [81, 32]	0.443
Pb+Pb $\to \Xi^-$	0−10%	$1.43 \pm 0.33 \pm 0.16$ [80, 81]	1.34
Pb+Pb $\to \Xi^-$	0−10%	$1.44 \pm 0.10 \pm 0.15$ [79, 81]	1.34
Pb+Pb $\to \overline{\Xi}^+$	0−10%	$0.31 \pm 0.03 \pm 0.03$ [79, 81]	0.443
Pb+Pb $\to \Omega^-$	0−5%	$0.31 \pm 0.07 \pm 0.05$ [81, 83]	0.246
Pb+Pb $\to \overline{\Omega}^+$	0−5%	$0.16 \pm 0.04 \pm 0.02$ [81, 83]	0.111
Pb+Pb $\to \Omega^-$	0−10%	$0.14 \pm 0.03 \pm 0.01$ [78, 81]	0.197
Pb+Pb $\to \overline{\Omega}^+$	0−10%	$0.07 \pm 0.03 \pm 0.01$ [78, 81]	0.071
Pb+Pb $\to \Omega^-$	0−11%	$0.259 \pm 0.037 \pm 0.026$ [81, 82]	0.197
Pb+Pb $\to \overline{\Omega}^+$	0−11%	$0.129 \pm 0.0122 \pm 0.013$ [81, 82]	0.071

The experimental data on midrapitity yieds of p, $\overline{p}$, strange Λ, $\overline{\Lambda}$ and multistrange $\Xi^-, \overline{\Xi}^+, \Omega^-$, and $\overline{\Omega}^+$, produced at different centralities in Pb+Pb collisions at 158 GeV/c per nucleon, measured by the NA49, NA57, and WA97 collaborations, together with the results of the QGSM calculations.

For secondary p, $\bar{p}$, and strange Λ and $\bar{\Lambda}$, one obtains a reasonable description of the experimental data, by using a value λ_s=0.32 for the strangeness suppression factor.

On the contrary, for the case of multistrange hyperon production of Ξ^-, $\bar{\Xi}^+$, Ω^-, and $\bar{\Omega}^+$, a correct description of the experimental data can only be obtained by taking significantly larger values of λ_s, i.e. by implementing a weaker suppression of the strangeness production.

This fact is a clear indication of a significant violation of the quark combinatorial rules.
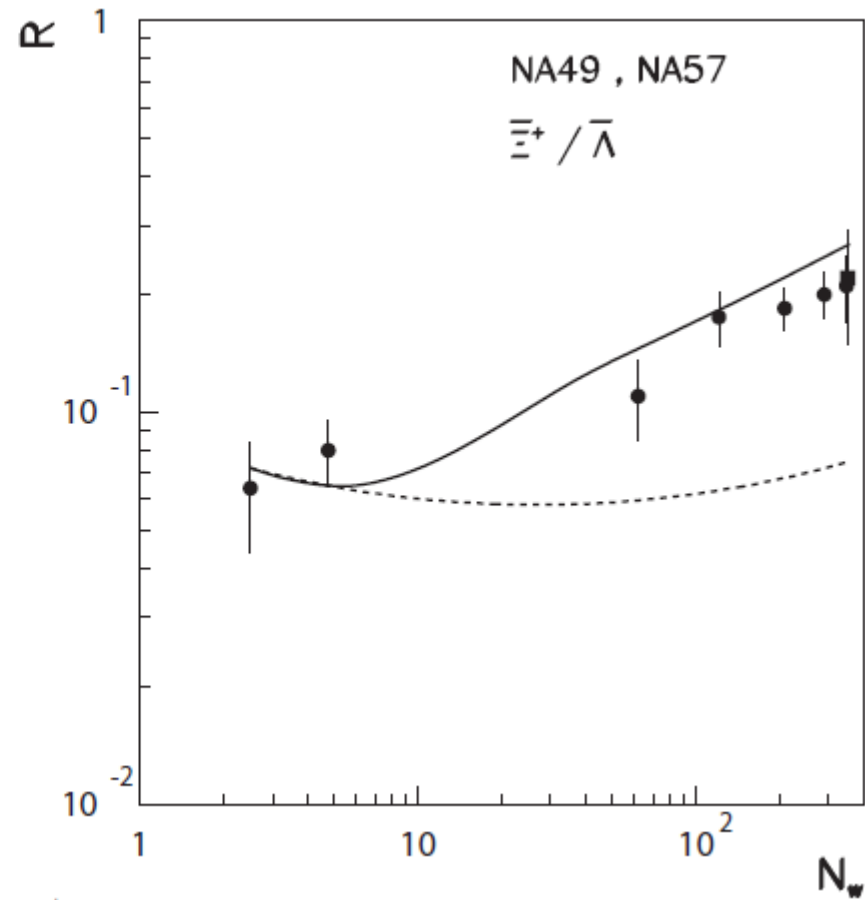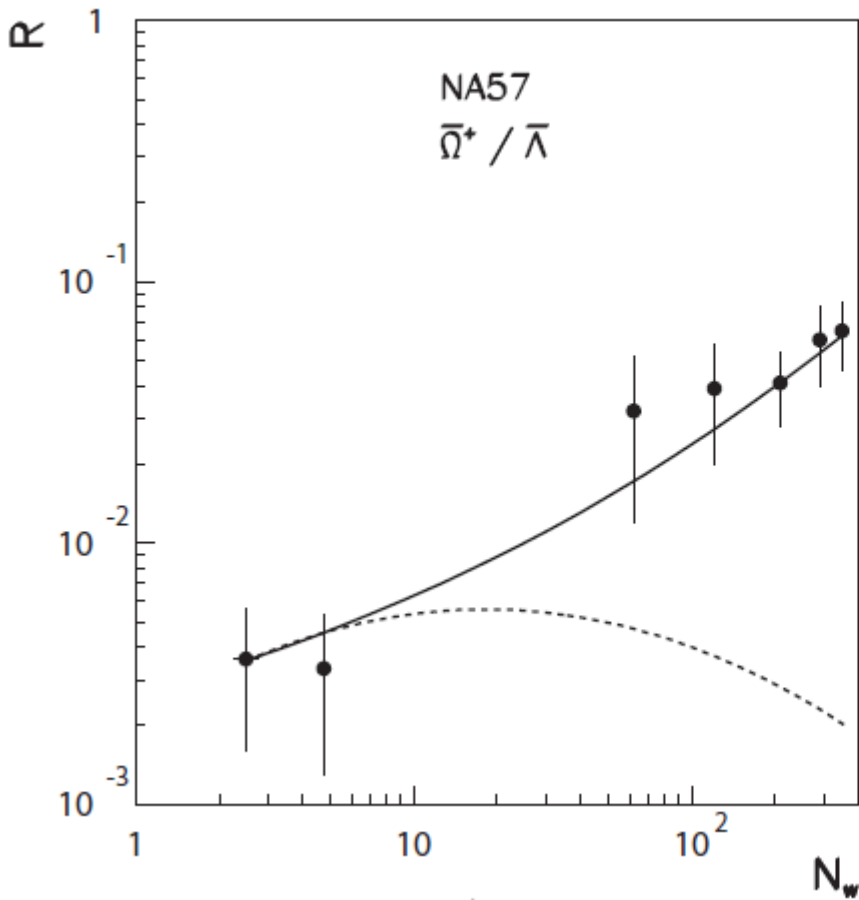
The ratios $\overline{\Omega}^+/\overline{\Lambda}$ (left panel) and $\overline{\Xi}^+/\overline{\Lambda}$ (right panel) as functions of the number of wounded nucleons, N_ω. The experimental data for *Pb+Pb* collisions for different values of N_ω (different centralities), measured by the NA57 Collaboration (points), and by the NA49 Collaboration (squares), are presented, and compared with the corresponding QGSM predictions.

Carlos Merino at HYP2022
14th International Conference on Hypernuclear and Strange Particle Physics
Prague, Czech Republic, June 29th, 2022

17/27

The necessity of using different values of the strangeness suppression factor λ_s to correctly describe the production, both of strange, and multistrange, hadrons at SPS, is made evident by the increase with centrality of the experimental ratios of the yields $\overline{\Omega}^+/\overline{\Lambda}$ and $\overline{\Xi}^+/\overline{\Lambda}$, measured in Pb+Pb collisions, since all other parameters in the model remain invariant.

When N_ω increases (centrality increases), the full line (increasing λ_s) also increases in agreement with the data, while the dashed line (constant λ_s), is mainly constant, and it shows a very significant disagreement with the esperimental data.

The difference between the full and dashed lines for the ratio $\overline{\Omega}^+/\overline{\Lambda}$ in a very central event is of about one order of magnitude.
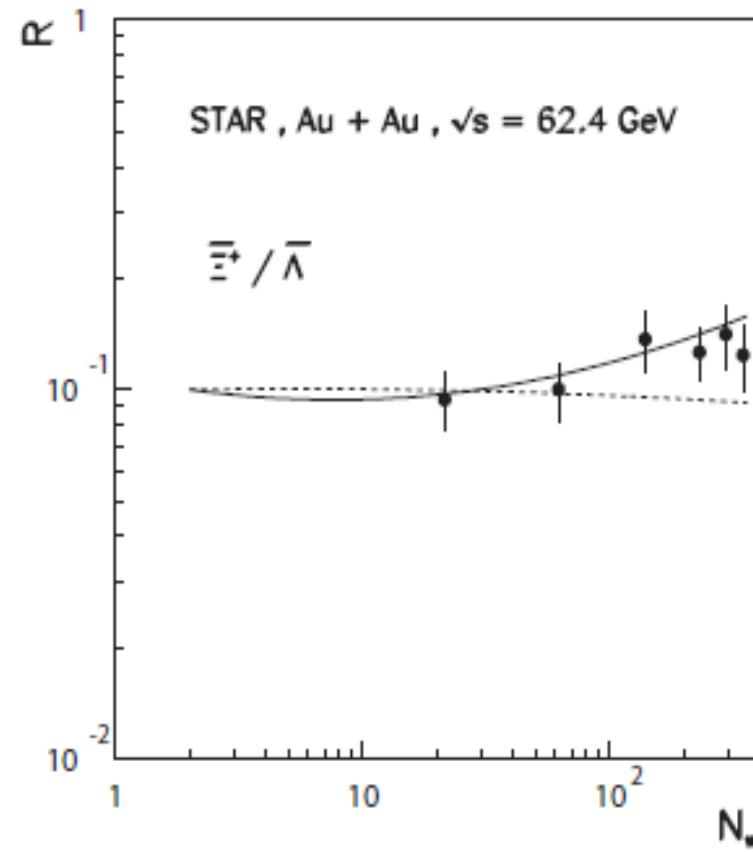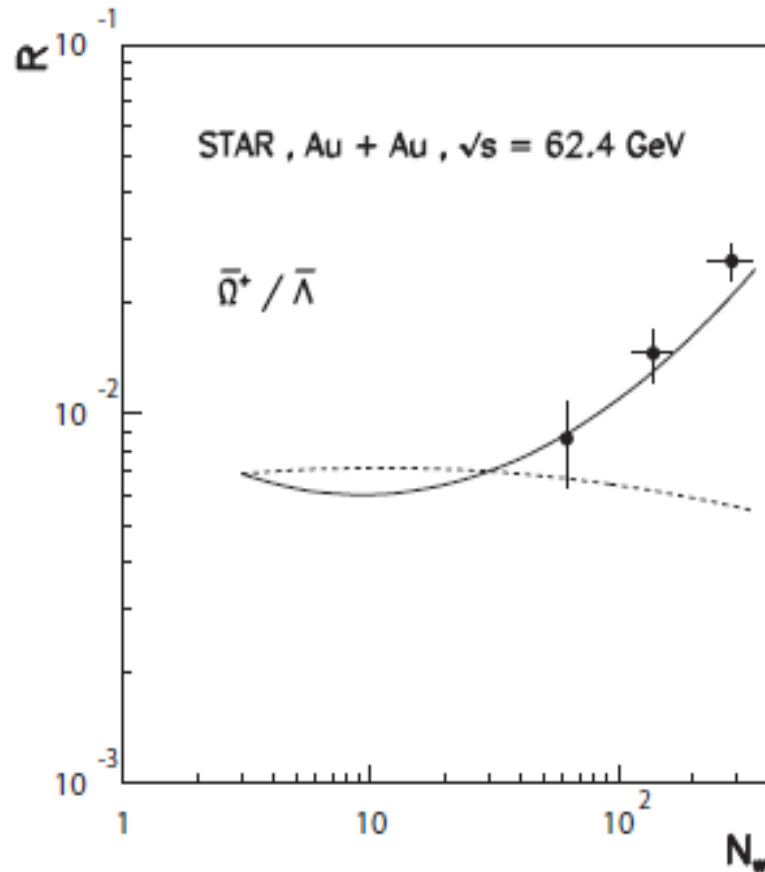
2. Star Collaboration Data

We consider the experimental data on midrapidity densities of protons and hyperons in Au+Au and Cu+Cu collisions, measured by the STAR (Phys. Rev. Lett. 108 (2012), 072301), and PHENIX (Phys. Rev. C69 (2004), 024904), collaborations at RHIC energies, and compare them with the corresponding QGSM results.

Carlos Merino at HYP2022
14th International Conference on Hypernuclear and Strange Particle Physics
Prague, Czech Republic, June 29th, 2022

19/27

Process	$\sqrt{s}$ (GeV)	Centrality	dn/dy (Experimental Data)	dn/dy (QGSM)	λ_s
Au+Au → p	62.4	0—5%	29.0 ± 3.8 [86]	22.826	0.32
Au+Au → $\bar{p}$	62.4	0—5%	13.6 ± 1.7 [86]	15.115	
Au+Au → Λ	62.4	0—5%	15.7 ± 0.3 ± 2.3 [87]	9.221	0.32
Au+Au → $\bar{\Lambda}$	62.4	0—5%	8.3 ± 0.2 ± 1.1 [87]	6.258	
Au+Au → Ξ^-	62.4	0—5%	1.63 ± 0.09 ± 0.18 [87]	1.406	0.4
Au+Au → $\bar{\Xi}^+$	62.4	0—5%	1.03 ± 0.00 ± 0.11 [87]	0.996	
Au+Au → Ω^-	62.4	0—20%	0, 212 ± 0.028 ± 0.018 [87]	0.222	0.55
Au+Au → $\bar{\Omega}^+$	62.4	0—20%	0, 167 ± 0.027 ± 0.015 [87]	0.154	
Au+Au → p	130.	0—5%	28.2 ± 3.1 [86]	27.450	0.32
Au+Au → p	130.	0—5%	28.7 ± 0.9 [90]	27.450	
Au+Au → $\bar{p}$	130.	0—5%	20.0 ± 2.2 [86]	22.723	
Au+Au → $\bar{p}$	130.	0—5%	20.1 ± 1.0 [90]	22.723	
Au+Au → Λ	130.	MB	4.8 ± 0.3 [89]	3.379	0.32
Au+Au → $\bar{\Lambda}$	130.	MB	4.3 ± 0.7 [89]	2.861	
Au+Au → Λ	130.	0—5%	17.3 ± 1.8 ± 2.8 [89]	13.070	0.32
Au+Au → Λ	130.	0—5%	17.0 ± 0.4 ± 1.7 [87]		
Au+Au → $\bar{\Lambda}$	130.	0—5%	12.7 ± 1.82 ± 2.0 [89]	11.053	
Au+Au → $\bar{\Lambda}$	130.	0—5%	12.3 ± 0.3 ± 1.2S [87]		
Au+Au → Ξ^-	130.	0—10%	2.0 ± 0.14 ± 0.2 [84]	1.976	0.39
Au+Au → $\bar{\Xi}^+$	130	0—10%	1.70 ± 0.12 ± 0.17 [84]	1.754	
Au+Au → $\Omega^- + \bar{\Omega}^+$	130.	0—10%	0.55 ± 0.11 ± 0.06 [84]	0.544	0.48
Cu+Cu → Λ	200	0—10%	4.68 ± 0.45 [88]	4.200	0.32
Cu+Cu → $\bar{\Lambda}$	200	0—10%	3.79 ± 0.37 [88]	3.772	
Cu+Cu → Ξ^-	200	0—10%	0.62 ± 0.08 [88]	0.559	0.33
Cu+Cu → $\bar{\Xi}^+$	200	0—10%	0.52 ± 0.08 [88]	0.507	
Cu+Cu → $\Omega^- + \bar{\Omega}^+$	200.	0—10%	0.141 ± 0.017 [88]	0.140	0.39
Au+Au → p	200.	0—5%	34.7 ± 4.4 [86]	31.450	0.32
Au+Au → $\bar{p}$	200.	0—5%	26.7 ± 3.4 [86]	27.765	
Au+Au → Λ	200	0—5%	14.8 ± 1.5 [88]	15.762	0.32
Au+Au → Λ	200	0—5%	16.7 ± 0.2 ± 1.1 [85]		
Au+Au → $\bar{\Lambda}$	200	0—5%	11.7 ± 0.9 [88]	14.152	
Au+Au → $\bar{\Lambda}$	200	0—5%	12.7 ± 0.2 ± 0.9 [85]		
Au+Au → Ξ^-	200	0—5%	2.17 ± 0.06 ± 0.19 [85]	2.173	0.34
Au+Au → $\bar{\Xi}^+$	200	0—5%	1.83 ± 0.05 ± 0.20 [85]	1.962	
Au+Au → $\Omega^- + \bar{\Omega}^+$	200.	0—5%	0.53 ± 0.04 ± 0.03 [85]	0.525	0.4

The experimental data on dn/dy by the STAR Collaboration, of p, $\bar{p}$, strange Λ, $\bar{\Lambda}$, and multistrange Ξ^-, $\bar{\Xi}^+$, Ω^-, and $\bar{\Omega}^+$ production, in central Au+Au and Cu+Cu collisions at RHIC energies, together with the results of the QGSM calculations.

The experimental points obtained by the STAR Collaboration on the ratios $\bar{\Omega}^+/\bar{\Lambda}$ (left panel) and $\bar{\Xi}^+/\bar{\Lambda}$ (right panel) in *Au+Au* collisions, at $\sqrt{s} = 62.4\ GeV$, at different centralities, as a function of the number of wounded nucleons, N_ω, and compared with the corresponding QGSM results.
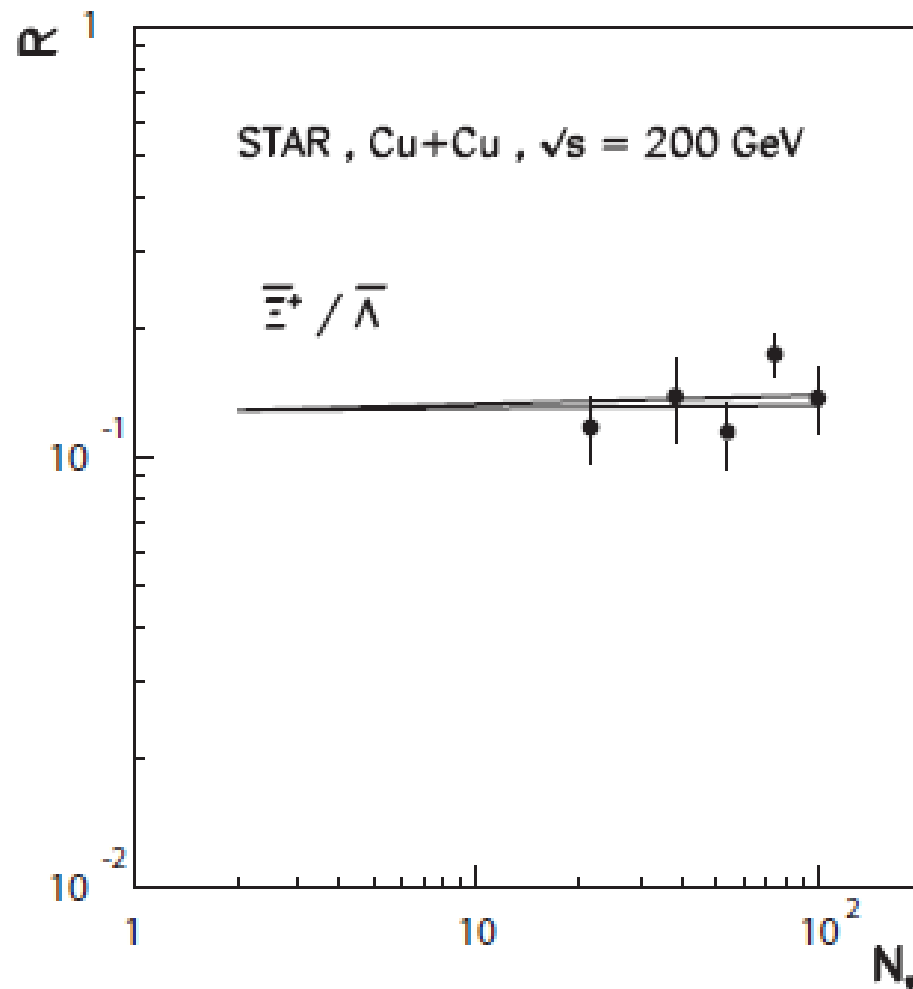
Carlos Merino at HYP2022
14th International Conference on Hypernuclear and Strange Particle Physics
Prague, Czech Republic, June 29th, 2022

21/27

The experimental points obtained by the STAR Collaboration on the ratio $\overline{\Xi}^+/\overline{\Lambda}$ in *Cu+Cu* collisions, at $\sqrt{s} = 200\ GeV$, at different centralities, as a function of the number of wounded nucleons, N_ω, and compared with the corresponding QGSM results.

Again, we see here that the value of the strangeness suppression factor λ_s for multistrange hyperon production is larger than for Λ and $\overline{\Lambda}$ production, though this difference is not so large as it is for collisions in the SPS energy range.

Moreover, it seems that the difference in the value of λ_s decreases with the growing of the energy, meaning that the violation of the quark combinatorial rules becomes less important for high energy collisions.

In particular, for the ratio $\overline{\Xi}^+/\overline{\Lambda}$ in *Cu+Cu* collisions, at $\sqrt{s} = 200\ GeV$, measured by the STAR Collaboration, the violation of the quark combinatorial rules decreases with the growth of the energy of the collision, the difference between the full (increasing λ_s), and the dashed (constant λ_s) lines being of the order of the experimental error bars.

Carlos Merino at HYP2022
14th International Conference on Hypernuclear and Strange Particle Physics
Prague, Czech Republic, June 29th, 2022

23/27

3. LHC Data

We consider the experimental data on p, $\bar{p}$, and Ξ^-, $\bar{\Xi}^+$, Ω^-, $\bar{\Omega}^+$ production, in central Pb+Pb collisions at $\sqrt{s} = 2.76\ TeV$, and of p+$\bar{p}$ production in central Pb+Pb collisions at $\sqrt{s} = 5.02\ TeV$, measured by the ALICE Collaboration (Phys. Rev. C88 (2013), 044910; Phys. Lett. B728 (2014), 216; Phys. Rev. C101 (2020), 044907), at the CERN LHC, and compare them with the corresponding QGSM results.

Carlos Merino at HYP2022
14th International Conference on Hypernuclear and Strange Particle Physics
Prague, Czech Republic, June 29th, 2022

24/27

Process	$\sqrt{s}$ (TeV)	Centrality	dn/dy (Experimental Data)	dn/dy (QGSM)	λ_s
Pb+Pb $\rightarrow p$	2.76	0–5%	34 ± 3 [91]	34.604	0,32
Pb+Pb $\rightarrow \bar{p}$	2.76	0–5%	33 ± 3 [91]	33.898	
Pb+Pb $\rightarrow p + \bar{p}$	5.02	0–5%	$74.56 \pm 0.06 \pm 3.75$ [93]	77.71	0,32
Pb+Pb $\rightarrow \Xi^-$	2.76	0–10%	$3.34 \pm 0.06 \pm 0.24$ [92]	3.357	0,32
Pb+Pb $\rightarrow \bar{\Xi}^+$	2.76	0–10%	$3.28 \pm 0.06 \pm 0.23$ [92]	3.317	
Pb+Pb $\rightarrow \Omega^-$	2.76	0–10%	$0,58 \pm 0.04 \pm 0.09$ [92]	0.606	0.38
Pb+Pb $\rightarrow \bar{\Omega}^+$	2.76	0–10%	$0,60 \pm 0.05 \pm 0.09$ [92]	0,601	

The experimental data on dn/dy by the ALICE Collaboration, of p, $\bar{p}$ central production at $\sqrt{s} = 2.76\ TeV$, of p+$\bar{p}$ central production at $\sqrt{s} = 5.02\ TeV$, and of $\Xi^-, \bar{\Xi}^+, \Omega^-, \bar{\Omega}^+$ production in central Pb+Pb collisions at $\sqrt{s} = 2.76\ TeV$ per nucleon, together with the results of the QGSM calculations.

We can see that the value of the strangeness suppression factor λ_s, for Ξ^- and $\bar{\Xi}^+$ production at LHC becomes smaller than at RHIC energies, taking at LHC the standard value $\lambda_s = 0.32$.

In the case of Ω^- and $\bar{\Omega}^+$ production, the value of λ_s also decreases with respect to the RHIC energy range.

Then, the unusually large values of λ_s for central Pb+Pb collisions at 158 GeV/c per nucleon (SPS), monotonically decrease with the growth of the initial energy of the collision (RHIC and LHC).

Thus, the experimental data seem to indicate a smaller increase of strangeness production at RHIC and LHC, when compared with that at SPS.

Conclusions

By comparing the QGSM predictions for strange and multistrange production in hadronic and nuclear collisions at high energies, we observe the following effect in the experimental data:

The experimental dependence on centrality of the ratios $\overline{\Omega}^+/\overline{\Lambda}$ and $\overline{\Xi}^+/\overline{\Lambda}$, in nuclear collisions at SPS energies, shows the dependence of the strangeness suppression factor, λ_s, on centrality.

On the contrary, the strangeness suppression parameter λ_s is constant for pp and light-nuclei collisions.

This effect, observed for heavy-ion collisions at SPS energies, disappears at very high (RHIC and LHC) energies.

Carlos Merino at HYP2022
14th International Conference on Hypernuclear and Strange Particle Physics
Prague, Czech Republic, June 29th, 2022

27/27